

Magnetic Position and Orientation Tracking System

FREDERICK H. RAAB, Member, IEEE
ERNEST B. BLOOD
TERRY O. STEINER
HERBERT R. JONES
Polhemus Navigation Sciences, Inc.

Abstract

Three-axis generation and sensing of quasi-static magnetic-dipole fields provide information sufficient to determine both the position and orientation of the sensor relative to the source. Linear rotation transformations based upon the previous measurements are applied to both the source excitation and sensor output vectors, yielding quantities that are linearly proportional to small changes in the position and orientation. Changes are separated using linear combinations of sensor output vectors, transformed to the desired coordinate frame, and used to update the previous measurements. Practical considerations for a head-tracking application are discussed.

Manuscript received December 10, 1978; revised January 15, 1979, March 22, 1979, and April 10, 1979.

Authors' address: Polhemus Navigation Sciences, Inc., A Subsidiary of The Austin Company, P.O. Box 298, Essex Junction, Vt 05452.

0018-9251/79/0900-0709 \$00.75 © 1979 IEEE

I. Introduction

Low-frequency quasi-static magnetic fields have been used in numerous short-range position and/or orientation measurement applications. Most of these techniques are based upon free-space field geometry, but others utilize the effects of a nearby conducting medium. A technique developed by Kalmus [1] uses phase-quadrature excitation of a two-axis magnetic-dipole source to determine the orientation of a two-axis sensor. A null-finding technique [2, 3] has been used to locate a buried vertical magnetic dipole for mine rescue and underground survey. The position and orientation of a buried magnetic dipole source can also be determined from the signals received by four or five three-axis sensors located at different positions on the surface [4, 5]. An electromagnetic channel guidance concept [6] uses a two-axis magnetic dipole source located on the Earth's surface. Several other techniques for the guidance of surface and sub-surface vehicles using the quasi-static fields surrounding long wires have also been devised [7, 8].

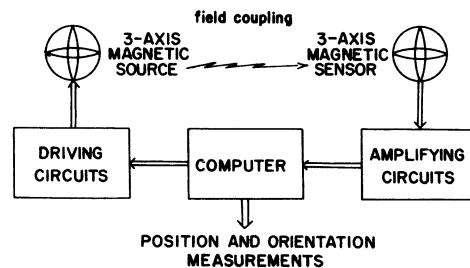


Fig. 1. System block diagram.

The system discussed here [9-12] used both a three-axis magnetic-dipole source and a three-axis magnetic sensor, along with the related electronic circuitry shown in Fig. 1. The excitation of the source and the resultant sensor output are represented as vectors; all source axes are to be excited simultaneously with signals of the same frequency and phase so that an equivalent single-axis source dipole of arbitrary orientation is produced. The source *excitation pattern* is composed of three sequential *excitation states*, each of which produces an *excitation vector* that is linearly independent from the other two. The resultant set of three sensor output vectors contains information sufficient to determine both the position and orientation of the sensor (6 degrees of freedom) relative to the source. Operation of the system is synchronous and under computer control.

This system *tracks* the position and orientation of the sensor by determining small changes in the coordinates and then updating the previous measurements. To accomplish this, the previous measurement is used to compute linear transformations that are approxi-

¹Variations are discussed in Section V of this paper.

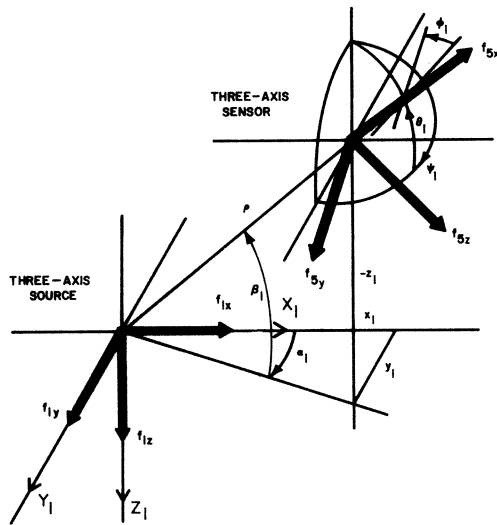


Fig. 2. Position and orientation coordinates.

mately the inverses of those describing the true source-to-sensor coupling. One set of such transformations is applied immediately prior to actual source excitation, while the other is applied to the sensor output vectors. The resultant transfer function is approximately that of a similarly aligned source and sensor. The set of processed output vectors differs from the specified source excitation vectors (prior to transformation) by quantities that are linearly proportional to the changes in position and orientation. Individual coordinate changes are extracted from linear combinations of the elements of the processed output vectors and subsequently transformed to the desired measurement coordinate frame.

The required transformations, detection equations, and coordinate conversions will be derived subsequently. However, it is first necessary to formulate the field coupling in matrix form and to establish a set of coordinate frames to facilitate the analysis.

II. Magnetic-Field Coupling

The first step in synthesizing a position-and-orientation-finding algorithm is the definition of coordinate frames and a vector-matrix formulation relating sensor output to source excitation.

Geometry

The geometric relationship between the three-axis source and the three-axis sensor is shown in Fig. 2. The *source coordinate frame* $X_1 - Y_1 - Z_1$ defined by the axes of source is used here as the reference for the final measurements. However, the source axes can be effectively aligned with any desired coordinate frame by altering the excitation. Similarly, coordinates

TABLE I
Coordinate Frame Definitions

Subscript	Name	Definition
0	Tracking	$f_0 = T_{\hat{\beta}_1} T_{\hat{\alpha}_1} f_1$
1	Source	Reference for other definitions.
2	Position	$f_2 = T_{\beta_1} T_{\alpha_1} f_1$
3	Sensor-position	$f_3 = \frac{C}{\rho^3} S f_2$
4	Zero-orientation sensor	$f_4 = T_{-\alpha_1} T_{-\beta_1} f_3$
5	Sensor-output	$f_5 = T_{\phi_1} T_{\theta_1} T_{\psi_1} f_4$
6	Derotated sensor	$f_6 = T_{-\hat{\psi}_1} T_{-\hat{\theta}_1} T_{-\hat{\phi}_1} f_5$
7	Restored tracking	$f_7 = T_{\hat{\beta}_1} T_{\hat{\alpha}_1} f_6$

Notes:

- 1) $\alpha_1, \beta_1, \rho, \psi_1, \theta_1, \phi_1$ represent true values.
 $\hat{\alpha}_1, \hat{\beta}_1, \hat{\rho}, \hat{\psi}_1, \hat{\theta}_1, \hat{\phi}_1$ represent previous estimates.
- 2) Symbols with a wavy underline correspond to boldface symbols in the text.

measured in the source coordinate frame can be converted to any desired coordinate frame mathematically.

The sensor position is specified in rectangular (x_1, y_1, z_1) or spherical $(\alpha_1, \beta_1, \rho)$ coordinates defined relative to the source coordinate frame. Sensor orientation is specified by a sequence of three rotations. Azimuthal rotation by ψ_1 first turns the sensor about its Z axis from $+X + Y$. The elevation rotation by θ_1 then turns the sensor about its Y_1 axis from $+X$ to $-Z$. Finally, a roll rotation by ϕ_1 turns the sensor about its X axis from $+Y$ to $+Z$. Note that in the zero-orientation condition, the three sensor axes are parallel to the corresponding source axes, and that the order of the rotations cannot be interchanged without changing the values of $\psi_1, \theta_1,$ and ϕ_1 . The subscript "1" denotes a coordinate referred to the source coordinate frame. Other numerical subscripts denote references to other coordinate frames (Table I) that are used in subsequent analyses.

Applications of this system use source and sensor loops whose diameters are small in comparison to the distance separating them. They can therefore be regarded as point sources and point sensors. The wavelength of the excitation signal is then long enough ($\rho \ll \lambda/2\pi$) that only the *near-field* or *quasi-static* field component (i.e., the term varying as the inverse-cube of distance) is significant.

Suppose now that the loop shown in Fig. 3 is excited with a current $i(t) = I \cos \omega t$. The magnetic field produced at a distance ρ and off-axis angle ξ is

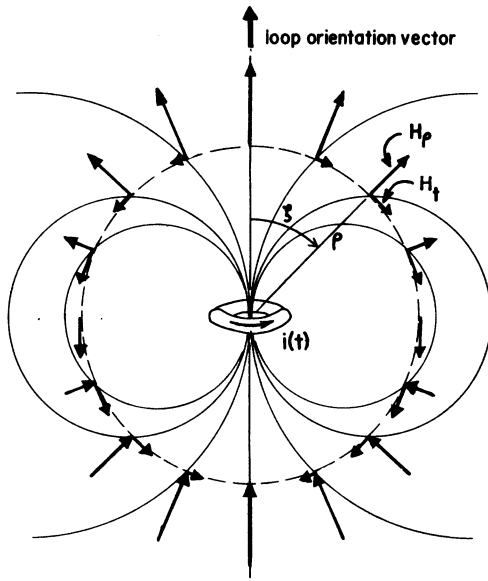


Fig. 3. Magnetic-dipole field.

described completely [13] by radial and tangential components

$$H_r = (M/2\pi q^3) \cos \zeta \quad (1)$$

and

$$H_t = [M/4\pi q^3] \sin \zeta \quad (2)$$

where $M = NIA$ is called the *magnetic moment* of the loop and A and N represent the area and number of turns of the loop. A temporal variation of $\exp(j\omega t)$ is implied; the spatial phase variation of $\exp(j\varrho/\lambda)$ can be neglected in this application. This characterization is valid for a loop of any shape as long as the distance is more than about four times the radius of the loop. Note that there is *no* frequency dependence in the amplitudes of the fields.

Source-Sensor Coupling

The excitation of a three-axis magnetic-dipole source and the resultant three-axis sensor output are most conveniently described in vector notation. The excitation of the source is therefore represented by $f_1 = [f_{1x}, f_{1y}, f_{1z}]^T$. The number of turns and area of the three source loops are assumed to be identical; hence f_{1x} , f_{1y} , and f_{1z} represent the amplitudes of the currents exciting the loops of X_1 axis, Y_1 axis, and Z_1 axis orientation, respectively.

Now let the output of a three-axis sensor be similarly represented by $f_3 = [f_{3x}, f_{3y}, f_{3z}]^T$, and consider the coupling between that sensor and a similarly aligned source f_2 . As depicted in Fig. 4, each source axis is coupled *only* to the corresponding sensor axis. Furthermore, since the $Y_2 - Y_3$ and $Z_2 - Z_3$ couplings are produced by *tangential* field components, their

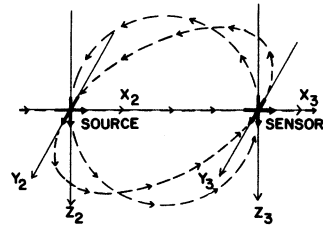


Fig. 4. Coupling between aligned source and sensor. Source, tracking, and sensor frames aligned.

TABLE II
Orthogonal Rotation Matrices

	Position	Orientation
<u>Azimuth</u> rotates X into Y	$T_\alpha = \begin{bmatrix} \cos \alpha & \sin \alpha & 0 \\ -\sin \alpha & \cos \alpha & 0 \\ 0 & 0 & 1 \end{bmatrix}$	$T_\psi = \begin{bmatrix} \cos \psi & \sin \psi & 0 \\ -\sin \psi & \cos \psi & 0 \\ 0 & 0 & 1 \end{bmatrix}$
<u>Elevation</u> rotates X into Z	$T_\beta = \begin{bmatrix} \cos \beta & 0 & -\sin \beta \\ 0 & 1 & 0 \\ \sin \beta & 0 & \cos \beta \end{bmatrix}$	$T_\theta = \begin{bmatrix} \cos \theta & 0 & -\sin \theta \\ 0 & 1 & 0 \\ \sin \theta & 0 & \cos \theta \end{bmatrix}$
<u>Roll</u> rotates Y into Z	$T_\gamma = \begin{bmatrix} 1 & 0 & 0 \\ 0 & \cos \gamma & \sin \gamma \\ 0 & -\sin \gamma & \cos \gamma \end{bmatrix}$	$T_\phi = \begin{bmatrix} 1 & 0 & 0 \\ 0 & \cos \phi & \sin \phi \\ 0 & -\sin \phi & \cos \phi \end{bmatrix}$

Notes:

- 1) $T_\alpha^{-1} = T_\alpha^T = T_{-\alpha}$, $T_\alpha T_\beta \neq T_\beta T_\alpha$, $T_{\beta'} T_{\beta''} = T_{\beta' + \beta''}$, etc.
- 2) Position roll is used only as a dummy variable and does not define sensor position or orientation.
- 3) Symbols with a wavy underline correspond to boldface symbols in the text.

amplitudes differ by a factor of $-\frac{1}{2}$ from the X_2 , $-X_3$ coupling which is produced by a *radial* field component. The coupling can be described completely in vector-matrix form by

$$f_3 = (C/q^3) S f_2 = (C/q^3) \begin{bmatrix} 1 & 0 & 0 \\ 0 & -1/2 & 0 \\ 0 & 0 & -1/2 \end{bmatrix} f_2 \quad (3)$$

where $C = NAG/2\pi$ incorporates sensor gain G and the common source factor $NA/2\pi$.

Effects of Position and Orientation

The coupling between a source and sensor of arbitrary position and orientation can be determined by inserting orthogonal rotation matrices [14] into (3). These matrices are based upon position azimuth and elevation (α_1 and β_1) and orientation azimuth, evaluation, and roll (ψ_1 , ϕ_1 , and θ_1), as shown in Table II.

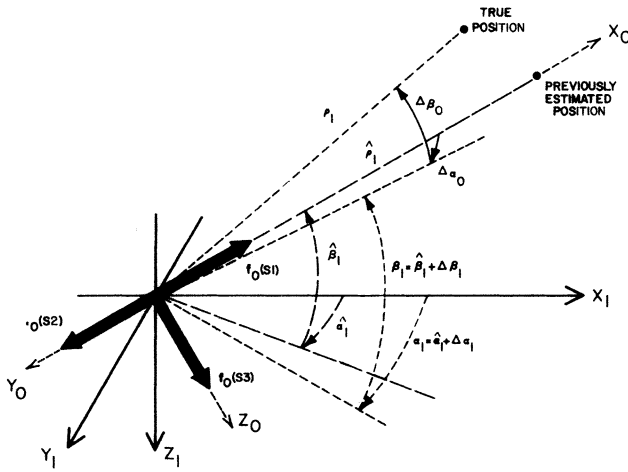


Fig. 5. True and previously measured position.

Note that the subscript defines both the type of transformation and its independent variable.

Consider first the coupling between the source and a zero-orientation sensor (whose output is f_4) located at $(\alpha_1, \beta_1, \varrho)$, as shown in Fig. 2. The excitation f_2 of an equivalent source whose X -axis is aligned with the line connecting the source and sensor can be determined by rotating the excitation vector of the real source by position azimuth and elevation, thus

$$f_2 = T_{\beta_1} T_{\alpha_1} f_1. \quad (4)$$

The coupling to a similarly aligned equivalent sensor f_3 then has the same form as (3), i.e., $f_3 = (C/\varrho^3) S f_2$. The output of the zero-orientation sensor is then found by applying inverse position rotations, thus

$$f_4 = (C/\varrho^3) T_{-\alpha_1} T_{-\beta_1} S T_{\beta_1} T_{\alpha_1} f_1 = (C/\varrho^3) Q f_1. \quad (5)$$

The equivalent sources and sensors used above are listed in Table I.

The output of the three-axis sensor of arbitrary orientation $(\psi_1, \theta_1, \phi_1)$ is determined by applying orientation azimuth, elevation, and roll rotations to the output of the equivalent zero-orientation sensor, thus

$$f_5 = T_{\phi_1} T_{\theta_1} T_{\psi_1} f_4 = (C/\varrho^3) A f_4 = (C/\varrho^3) A Q f_1. \quad (6)$$

These expressions will be used subsequently to derive the position-and-orientation-finding algorithm.

III. Determination of Position and Orientation Changes

The matrix multiplications in (6) imply source-to-sensor coupling equations that contain multiple trigonometric products and sums. These nonlinear coupling equations can be reduced to linearized equations in small changes in the position and orientation

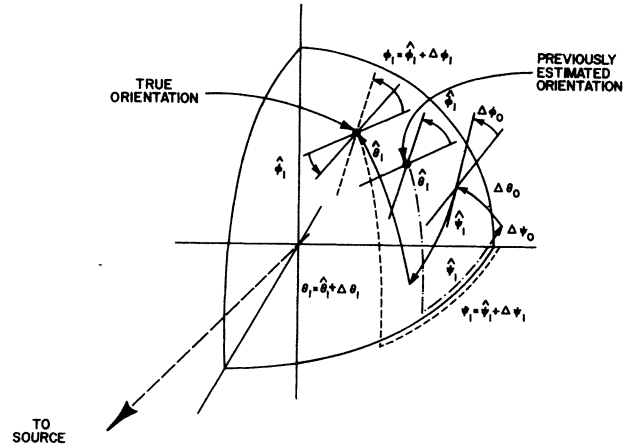


Fig. 6. True and previously measured orientation.

of the sensor. This is accomplished by using the previous measurements of position and orientation to compute rotation matrices that approximately undo the effects of the (large-angle) sensor position and orientation.

Use of Previous Measurements

The relationship of the true sensor position $(\alpha_1, \beta_1, \varrho)$ to the previously estimated sensor position $(\hat{\alpha}_1, \hat{\beta}_1, \hat{\varrho})$ is illustrated in Fig. 5; note that both positions are defined in source-frame coordinates. The differences in the source-frame position angles can be represented by $\Delta\alpha_1$ and $\Delta\beta_1$; hence $\alpha_1 = \hat{\alpha}_1 + \Delta\alpha_1$ and $\beta_1 = \hat{\beta}_1 + \Delta\beta_1$. The difference in the position angles can also be defined by angles $\Delta\alpha_0$ and $\Delta\beta_0$, which are referenced to the *tracking coordinate frame* $X_0, -Y_0, -Z_0$. The tracking frame is defined by rotations from the source coordinate frame $X_1 - Y_1 - Z_1$ by previously estimated position azimuth $\hat{\alpha}_1$ and elevation $\hat{\beta}_1$. Differences between estimated and true orientation angles can similarly be defined relative to either the source-frame or tracking frame, as shown in Fig. 6.

Now consider an equivalent source excitation vector f_0 specified in the tracking frame. This vector is converted to the true source excitation vector f_1 by inverse rotations by estimated elevation and azimuth; thus

$$f_1 = T_{-\hat{\alpha}_1} T_{-\hat{\beta}_1} f_0. \quad (7)$$

Combining this with (6) and (5) yields

$$\begin{aligned} f_5 &= (C/\varrho^3) A T_{-\alpha_1} T_{-\beta_1} S (T_{\beta_1} T_{\alpha_1} T_{-\hat{\alpha}_1} T_{-\hat{\beta}_1}) f_0 \\ &= (C/\varrho^3) A T_{-\alpha_1} T_{-\beta_1} S \Delta P f_0. \end{aligned} \quad (8)$$

If there has been no movement of the sensor since the previous estimate of position was made, $\alpha_1 = \hat{\alpha}_1$ and $\beta_1 = \hat{\beta}_1$, hence $T_{\beta_1} T_{\alpha_1} T_{-\hat{\alpha}_1} T_{-\hat{\beta}_1} = I$. It is therefore

necessary for that sequence of rotations to reduce to a differential rotation ΔP when the changes in position are small.

The nature of the differential rotation matrix ΔP can be determined in two ways. Direct reduction of (8) yields the source-frame formulation

$$\begin{aligned}\Delta P &= T_{\beta_1} T_{-\alpha_1} (T_{-\hat{\alpha}_1} T_{-\hat{\beta}_1}) \\ &\cong T_{\beta_1} T_{\alpha_1} (T_{-\alpha_1} T_{\Delta\alpha_1} T_{-\beta_1} T_{-\beta_1} T_{\Delta\beta_1}) \\ &= T_{\beta_1} T_{\Delta\alpha_1} T_{-\beta_1} T_{\Delta\beta_1}\end{aligned}$$

$$= \begin{bmatrix} 1 & \Delta\alpha_1 \cos \beta_1 & -\Delta\beta_1 \\ -\Delta\alpha_1 \cos \beta_1 & 1 & -\Delta\alpha_1 \sin \beta_1 \\ \Delta\beta_1 & \Delta\alpha_1 \sin \beta_1 & 1 \end{bmatrix}. \quad (9)$$

However, it is more convenient to equate the true position transformation $T_{\beta_1} T_{\alpha_1}$ to the estimated position transformation followed (premultiplied) by a sequence of differential rotations, thus

$$\begin{aligned}\Delta P &= [T_{\beta_1} T_{\alpha_1}] T_{-\alpha_1} T_{-\beta_1} \\ &\cong [(T_{\Delta\gamma_0} T_{\Delta\beta_0} T_{\Delta\alpha_0}) T_{\beta_1} T_{\alpha_1}] T_{-\alpha_1} T_{-\beta_1} \\ &= T_{\Delta\gamma_0} T_{\Delta\beta_0} T_{\Delta\alpha_0} = \begin{bmatrix} 1 & \Delta\alpha_0 & -\Delta\beta_0 \\ -\Delta\alpha_0 & 1 & \Delta\gamma_0 \\ \Delta\beta_0 & -\Delta\gamma_0 & 1 \end{bmatrix}. \quad (10)\end{aligned}$$

Note that the differential angles $\Delta\alpha_0$, $\Delta\beta_0$, and $\Delta\gamma_0$ are referenced to the tracking coordinate frame. The inclusion of a roll rotation ($T_{\Delta\gamma_0}$) is necessary to allow for the misalignment of coordinate axes when the same position is obtained by two different sequences of rotations. However, position roll is not an independent variable, and its effects are subsequently shown to be cancelled and not directly observable.

The application of preexcitation transformations therefore reduces the large-angle transformations on the right side of S in (8) to small-angle transformations. The large-angle transformation on the left side of S can similarly be reduced to small-angle transformations by applying inverse transformations (based upon estimated position and orientation) to the sensor output vector f_s . To do this, a *restored tracking frame* equivalent output vector f_7 is defined by

$$f_7 = T_{\beta_1}^* T_{\hat{\alpha}_1}^* A^{-1} f_s = T_{\beta_1}^* T_{\hat{\alpha}_1}^* T_{-\hat{\psi}_1} T_{-\hat{\theta}_1} T_{-\hat{\phi}_1} f_s. \quad (11)$$

The above transformations produce a differential rotation matrix which must reduce to $(\Delta P)^{-1}$ in the absence of orientation errors; hence

$$(T_{\hat{\beta}_1} T_{\hat{\alpha}_1} \hat{A}^{-1})(A T_{-\alpha_1} T_{-\beta_1}) \cong (\hat{A}^{-1} A)(\Delta P)^{-1} = \Delta A (\Delta P)^{-1}. \quad (12)$$

Rearrangement of the above yields

$$(\hat{A} T_{-\hat{\alpha}_1} T_{-\hat{\beta}_1}) [\Delta A (\Delta P)^{-1}] = A T_{-\alpha_1} T_{-\beta_1} \quad (13)$$

hence the differential orientation rotation ΔA is based upon tracking-frame orientation angles (Fig. 6) and

$$\Delta A = T_{\Delta\psi_0} T_{\Delta\theta_0} T_{\Delta\phi_0} = \begin{bmatrix} 1 & \Delta\psi_0 & -\Delta\theta_0 \\ -\Delta\psi_0 & 1 & \Delta\phi_0 \\ \Delta\theta_0 & -\Delta\phi_0 & 1 \end{bmatrix}. \quad (14)$$

Substitution of (14) and (8) into (10) now produces

$$f_7 = (C/\rho^3) \Delta A (\Delta P)^{-1} S \Delta P f_0 = (C/\rho^3) R f_0 \quad (15)$$

where

$$R = \begin{bmatrix} 1 & \frac{3}{2}\Delta\alpha_0 - \frac{1}{2}\Delta\psi_0 & -\frac{3}{2}\Delta\beta_0 + \frac{1}{2}\Delta\theta_0 \\ \frac{3}{2}\Delta\alpha_0 - \Delta\psi_0 & -\frac{1}{2} & -\frac{1}{2}\Delta\phi_0 \\ -\frac{3}{2}\Delta\beta_0 + \Delta\theta_0 & \frac{1}{2}\Delta\phi_0 & -\frac{1}{2} \end{bmatrix}. \quad (16)$$

The preexcitation, true position and orientation, field-coupling, and post-sensing transformation sequence is shown in Fig. 7. Note that all large-angle effects have been reduced to small-angle effects and replaced by small-angle approximations; position roll ($\Delta\gamma_0$) has disappeared. The transfer function between a tracking-frame vector f_0 and a restored tracking-frame vector f_7 is therefore linear in small changes in position and orientation. Furthermore, the changes are readily identifiable in tracking-frame coordinates.

Excitation States

Determination of position and orientation requires sensor outputs corresponding to three linearly independent source-excitation vectors. The source and sensor vectors produced during different excitation states are denoted by an attached parenthesized *excitation-state symbol*. The three source excitation vectors used here correspond to the tracking-frame axes:

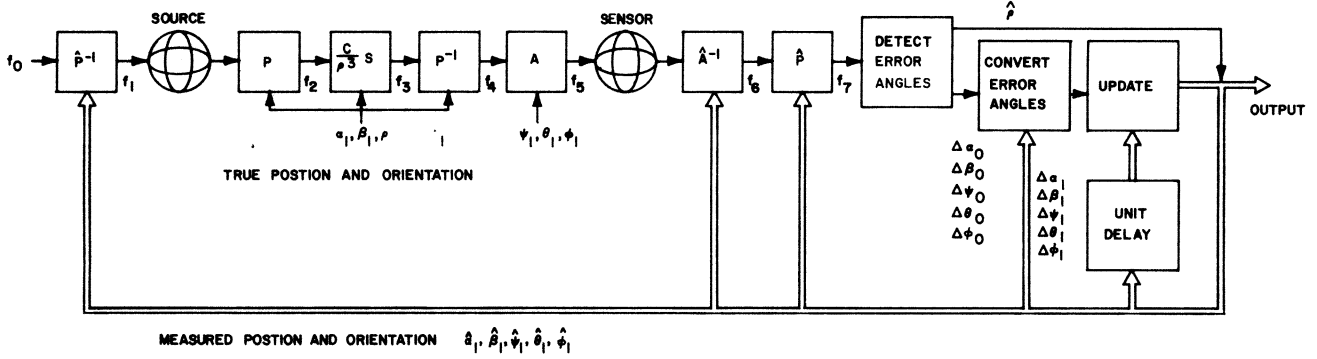


Fig. 7. Processing sequence.

$$f_0(S1) = \begin{bmatrix} 1 \\ 0 \\ 0 \end{bmatrix}, f_0(S2) = \begin{bmatrix} 0 \\ 1 \\ 0 \end{bmatrix}, \text{ and } f_0(S3) = \begin{bmatrix} 0 \\ 0 \\ 1 \end{bmatrix}. \quad (17)$$

A set of three excitation vectors constitutes an *excitation pattern*. The use of other excitation patterns containing more excitation vectors is readily related to the use of the above three-state pattern by linear transformation.

The restored tracking-frame sensor response vectors corresponding to the tracking-frame excitation vectors of (17) correspond to the columns of matrix R in (16); i.e.,

$$f_r(S1) = (C/\hat{\rho}^3) \begin{bmatrix} 1, & \frac{3}{2}\Delta\alpha_0 - \Delta\psi_0, & -\frac{3}{2}\Delta\beta_0 + \Delta\theta_0 \end{bmatrix}^T \quad (18)$$

$$f_r(S2) = (C/\hat{\rho}^3) \begin{bmatrix} \frac{3}{2}\Delta\alpha_0, & -\frac{1}{2}\Delta\psi_0, & -\frac{1}{2}, & \frac{1}{2}\Delta\phi_0 \end{bmatrix}^T \quad (19)$$

$$f_r(S3) = (C/\hat{\rho}^3) \begin{bmatrix} -\frac{3}{2}\Delta\beta_0, & \frac{1}{2}\Delta\theta_0, & \frac{1}{2}\Delta\phi_0, & -\frac{1}{2} \end{bmatrix}^T. \quad (20)$$

The first unknown to be estimated is distance, since it is given explicitly by the amplitudes of the constant terms in (18), (19), and (20):

$$\hat{\rho} = \sqrt[3]{C/f_{7x}(S1)} = \sqrt[3]{-C/2f_{7y}(S2)} = \sqrt[3]{-C/2f_{7z}(S3)} \quad (21)$$

The factor $C/\hat{\rho}^3$ is then computed,² and the five error angles are determined from linear combinations of the nine quantities in (18), (19), and (20):

² If the constant C is unknown, an invalid range estimate will be determined; however, determination of the error angles is unaffected.

$$\Delta\alpha_0 = \frac{2}{3}(\hat{\rho}^3/C)[2f_{7x}(S2) - f_{7y}(S1)] \quad (22)$$

$$\Delta\beta_0 = \frac{2}{3}(\hat{\rho}^3/C)[f_{7z}(S1) - 2f_{7x}(S3)] \quad (23)$$

$$\Delta\psi_0 = 2(\hat{\rho}^3/C)[f_{7x}(S2) - f_{7y}(S1)] \quad (24)$$

$$\Delta\theta_0 = 2(\hat{\rho}^3/C)[f_{7z}(S1) - f_{7x}(S3)] \quad (25)$$

$$\Delta\phi_0 = 2(\hat{\rho}^3/C)f_{7x}(S2) = -2(\hat{\rho}^3/C)f_{7y}(S3). \quad (26)$$

Linear combinations of elements can be used to minimize the effects of noise upon the range and roll estimates. This operation is represented by the "error detection" block in Fig. 7.

Error-Angle Coordinate-Frame Conversion

While the range estimate $\hat{\rho}$ is universal to all coordinate frames, the error angles ($\Delta\alpha_0, \Delta\beta_0, \Delta\psi_0, \Delta\theta_0, \Delta\phi_0$) are referenced to the tracking frame. Before they can be used to update the previous source-frame measurements of position and orientation, they must be converted to source-frame error angles ($\Delta\alpha_1, \Delta\beta_1, \Delta\psi_1, \Delta\theta_1, \Delta\phi_1$). This operation follows the error-detection block in Fig. 7.

The method of conversion of the position error angles $\Delta\alpha_0$ and $\Delta\beta_0$ to $\Delta\alpha_1$ and $\Delta\beta_1$ is most readily derived by equating ΔP as given by (9) and (10). If $|\beta_1| \neq \pi/2$, this produces

$$\Delta\alpha_1 = \Delta\alpha_0/\cos\beta_1 \quad (27)$$

and

$$\Delta\beta_1 = \Delta\beta_0. \quad (28)$$

Modified conversion formulas must be used when $\beta_1 \cong \pm \pi/2$.

The equations that convert tracking-frame orientation errors to source-frame orientation errors can similarly be derived by substituting $\psi_1 = \hat{\psi}_1 + \Delta\psi_1$, $\theta_1 = \hat{\theta}_1 + \Delta\theta_1$, and $\phi_1 = \hat{\phi}_1 + \Delta\phi_1$ into (12) and (13), producing

$$\begin{aligned}
& T_{\hat{\phi}_1 + \Delta\phi_1} T_{\hat{\theta}_1 + \Delta\theta_1} T_{\hat{\psi}_1 + \Delta\psi_1} T_{-\hat{\alpha}_1} T_{-\hat{\beta}_1} \\
&= T_{\hat{\phi}_1} T_{\hat{\theta}_1} T_{\hat{\psi}_1} T_{-\hat{\alpha}_1} T_{-\hat{\beta}_1} (T_{\Delta\phi_0} T_{\Delta\theta_0} T_{\Delta\psi_0}). \quad (29)
\end{aligned}$$

Note that in (29) position angle estimates have been set equal to true position angles, since the differential position angles do not affect the differential orientation angles ($\Delta\phi_1, \Delta\alpha_1 \cong 0$, etc.). However, the tedious reduction required can be avoided by observing [14] that a differential angle (angle rate) is transformed from one coordinate frame to another as is a coordinate of the axis about which the differential angle produces rotation. To visualize this, consider that both $\Delta\alpha$ and z are invariant under azimuthal rotation T_α .

Premultiplying (29) by $T_{-\hat{\theta}_1} T_{-\hat{\phi}_1}$ and some rearrangement yields

$$\begin{aligned}
& T_{-\hat{\theta}_1} T_{\Delta\phi_1} T_{\hat{\theta}_1} T_{\Delta\theta_1} T_{\Delta\psi_1} T_{\hat{\psi}_1} T_{-\hat{\alpha}_1} T_{-\hat{\beta}_1} \\
&= T_{\hat{\psi}_1 - \hat{\alpha}_1} T_{-\hat{\beta}_1} T_{\Delta\phi_0} T_{\Delta\theta_0} T_{\Delta\psi_0}. \quad (30)
\end{aligned}$$

Vectors of differential angles are now formed by placing the angle errors in the elements corresponding to their axes of rotation (e.g., $[\Delta\phi_0, \Delta\theta_0, \Delta\psi_0]^T$). Since differential angles are subjected to only those transformations occurring to their *left* in (30) and since $\Delta\phi_1$ is subjected to a rotation by $-\hat{\theta}_1$, while $\Delta\theta_1$ and $\Delta\psi_1$ are subjected to rotations by both $-\hat{\theta}_1$ and $+\hat{\theta}_1$, the differential-angle conversion equation has the form

$$\begin{aligned}
& \begin{bmatrix} \Delta\phi_1 \cos \hat{\theta}_1 \\ \Delta\theta_1 \\ \Delta\psi_1 - \Delta\phi_1 \sin \hat{\theta}_1 \end{bmatrix} \\
&= T_{-\hat{\theta}_1} \begin{bmatrix} \Delta\phi_1 \\ 0 \\ 0 \end{bmatrix} + \begin{bmatrix} 0 \\ \Delta\theta_1 \\ \Delta\psi_1 \end{bmatrix} = T_{\hat{\psi}_1 - \hat{\alpha}_1} T_{-\hat{\beta}_1} \begin{bmatrix} \Delta\phi_0 \\ \Delta\theta_0 \\ \Delta\psi_0 \end{bmatrix}. \quad (31)
\end{aligned}$$

Updating and Acquisition

The source-frame position and orientation error angles are now used to update the previous measurements by simple addition; i.e., $\hat{\alpha}_1 + \Delta\alpha_1 \rightarrow \hat{\alpha}_1$, etc. Initially (or after a loss of power or signal), the tracking system must *acquire* approximately correct measurements in order to track properly. Since the transformations used are based upon small-angle approxima-

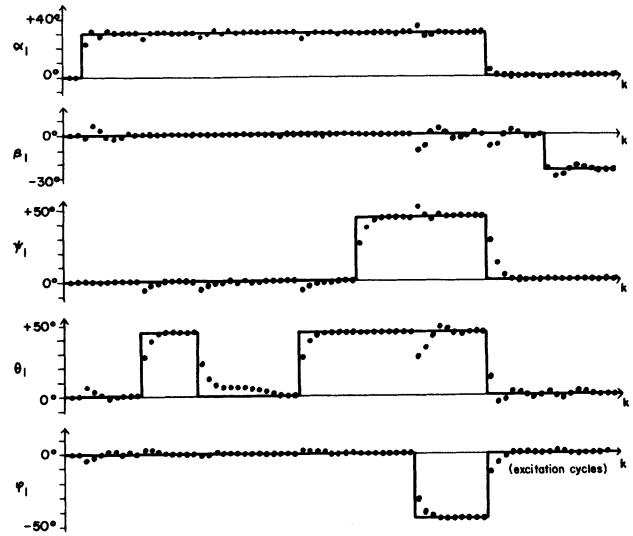


Fig. 8. Responses to large-angle errors. Solid lines indicate true values (inputs) and dots indicate measured values (outputs).

tions, the magnitudes of the measured errors are incorrect if the true angular errors are large. However, the polarities (signs) of the errors are correct, and this allows the system to achieve proper tracking within a few iterations after the occurrence of a large angular error (Fig. 8). The system contains one inherent 180° ambiguity³ that is in general resolved through “common sense” about realistic positions and orientations.

IV. Application Considerations

Magnetic tracking systems have been used in a number of helmet-mounted sight (HMS) applications to measure the orientation of the helmet and consequently its wearer’s line-of-sight. An HMS system can, for example, enable the pilot of a fighter aircraft to transfer a visually acquired target to an electronic tracking system. The line-of-sight to a target acquired by an electronic system or one crew member can be transferred to another crew member’s vision by a cueing display that indicates the direction in which to look. By slaving a range-measuring radar to the line-of-sight specified by an HMS, the relative position of a visually acquired target can be determined. This information can also be used to facilitate search-and-rescue operations by combining it with true position (measured by a navigation system) to map automatically the area that has been searched. The HMS application illustrates several practical considerations relating to the magnetic tracking system.

³For example, the signals for $\alpha_1 = \beta_1 = \psi_1 = \theta_1 = \phi_1 = 0$ are indistinguishable from those for $\beta_1 = \theta_1 = \phi_1 = 0$ and $\alpha_1 = \psi_1 = 180^\circ$.

Configuration

In an HMS application, the three-axis sensor is mounted on the helmet and the three-axis source is mounted above and behind the nominal head position on a nonmetallic structure such as the aircraft canopy. The helmet is equipped with a collimated (focused-at-infinity) reticle that is used to sight the target and optionally equipped with a cueing display. Sensor mounting is noncritical because the system is initialized by "bore sighting" in which the system derives a rotation sequence that aligns the sensor with the aircraft reference frame. The source and the sensor are typically separated by a range of a few centimeters to one meter.

The sensor is connected to the system control panel through a cable roughly three meters in length. There the three sensor outputs are preamplified, multiplexed, and transmitted to the system electronics unit. The multiplexed signals are then synchronously demodulated and digitized by a 12-bit analog-to-digital converter. The source of driving signals are generated in the system electronics unit; their instantaneous amplitudes are produced by 12-bit multiplying digital-to-analog converters controlled by the computer. Stepped automatic gain control is included in both the source and sensor circuits to reduce dynamic range requirements.

Carrier frequencies are typically in the 7- to 14-kHz range, and the choice of a carrier frequency represents a compromise between equipment complexity, sensitivity, noise, and source inductance. The excitation pattern and associated processing leading to updated measurements are repeated typically at 30- to 120-Hz rates. These rates are limited by computation time, source inductance (response time), noise, and allowable source moment.

Since the sensor must be both small and lightweight, yet must deliver a signal sufficient to allow (in this application) 12-bit accuracy (1 part in 4096), it generally imposes the most severe design constraints upon the system. Both the sensor and the source are wound on ferrite cores to increase their effective areas (sensitivity) by factors of 2 to 3.5, depending on the particular core shape. In the example HMS application, the sensor is roughly $1.3 \text{ cm} \times 1.9 \text{ cm} \times 2.6 \text{ cm}$, while the source is roughly 2.5 cm on each side. The source magnetic moment is approximately $0.086 \text{ At} \cdot \text{m}^2$ when driven by a peak current of 200 mA. The sensor produces an output of approximately $0.12 \text{ V}/(\text{At}/\text{m})$.

Source and Sensor Imperfections

The imperfections in the three-axis source and sensor can be described by 3×3 fixed-valued matrices that include both rotation (due to physical mounting of the source or sensor), gain, and skewing

(due to cross coupling between axes). The elements of the sensor sensitivity matrix can be determined by measuring its responses (on all three axes) to three orthogonal fields produced by a Helmholtz coil. The elements of the source matrix can similarly be measured by exciting its three axes in each of three orientations and measuring the responses in the Helmholtz coil. Inclusion of the inverses of these matrices in the computations then removes the measured imperfections. This can be done either in the hardware by cross-coupling in the source-driving circuitry or in the software by insertion of the inverse sensitivity matrix before \hat{A}^{-1} in Fig. 7.

Nearby Metallic Structure

A magnetic system is often required to operate in an environment containing metallic structures that produce scattering (distortion) of its magnetic-dipole fields, hence significant measurement errors. Ferromagnetic material can alter the shape of any magnetic field. The ac magnetic fields used in the HMS system produce circulating (eddy) currents in nearby conductive material thereby generating secondary ac magnetic fields and distorting the field pattern.

The complexity of the metallic structure in general precludes analytical prediction of the scattered fields (and makes numerical prediction difficult). A useful limit can be obtained by assuming that an infinite conducting plane produces as much or more field distortion as would any object at the same distances from the source and sensor. By using simple image theory, the conducting plane can be replaced with an image source; the ratio of the free-space and scattered fields is then estimated to be the ratio of the inverse cubes of the distances from the sensor to the source and to its image. This produces a rule of thumb stating that an object whose distance from the source is at least twice the distance separating the source and sensor produces a scattered field whose magnitude is 1 percent or less of the magnitude of the desired field.

Metallic structure that is fixed in position and orientation with respect to the source produces field distortion that is constant at any given position. Compensation for the field distortion is therefore possible as long as the fields at each allowed position are unique and span three-dimensional vector space (i.e., the field vectors produced by the three source excitation states are linearly independent). Corrections can take the form of additive vectors or a sequence of rotations, and can be stored in either a look-up table or as polynomials in the position parameters.

Variations

Three other multiaxis magnetic position and orientation measurement concepts provide flexibility for

varied applications. The first uses a fixed source-frame excitation pattern. The preexcitation and post-sensing rotations described here are then applied to a 3×3 matrix formed by assembling the true sensor output vectors, producing a 3×3 matrix of the sensor output vectors of the tracking system. The second concept [15] uses squared vector magnitudes and dot products to determine position and orientation through direct, closed-form computations. The third concept [16] uses two three-axis ferrite antennas alternately as sources and sensors, thereby enabling two separate units to determine their relative positions and orientations.

Acknowledgment

This paper describes a position and orientation measurement concept invented by J. Kuipers [10-12] and provides a detailed analysis of the concept using the inventor's system model illustrated in Fig. 7. A.R. DeRuyck and A.G. Rodgers played significant roles in the development and testing of related hardware.

References

- [1] H.P. Kalmus, "A new guiding and tracking system," *IRE Trans. Aerosp. Navig. Electron.*, vol. 9, pp. 7-10, Mar. 1962.
- [2] J.H. Murphy and H.E. Parkinson, "Underground mine communications," *Proc. IEEE*, vol. 66, pp. 26-50, Jan. 1978.
- [3] R.G. Olsen and A.J. Farstad, "Electromagnetic direction finding experiments for location of trapped miners," *IEEE*

- Trans. Geosci. Electron.*, vol. GE-11, pp. 178-185, Oct. 1973.
- [4] T.W.H. Caffey, "Locating a buried Earth penetrator," Sandia Laboratories, Albuquerque, N. Mex., Rep. SAND77-0646, Nov. 1977.
- [5] T.W.H. Caffey, "Locating a buried magnetic dipole," *Proc. Electromagnetic Guided Waves Workshop*, Boulder, Colo., Mar. 28-30, 1978.
- [6] G.S. Barta and R.G. Olsen, "A short-range VLF navigation system for rivers and harbors," *IEEE Antenna and Propagation Soc. Internatl. Symp. 1977*, Stanford, Calif., pp. 124-127, June 20-22, 1977.
- [7] J.C. Coyne, F.J. Elia, and H. Southworth, Jr., "Location detection and guidance systems for burrowing device," U.S. Patent 3 529 682, Sept. 22, 1970.
- [8] T. Gullich, "Indicator," U.S. Patent 3 777 304, Dec. 4, 1973.
- [9] A.R. DeRuyck and J. Kuipers, "An electromagnetic position sensor," Polhemus Navigations Sciences, Inc., Burlington, Vt., Tech. Rep. AFAL-TR-73-281, Nov. 30, 1973.
- [10] J. Kuipers, "Object tracking and orientation determination means, system, and process," U.S. Patent 3 868 565, Feb. 25, 1975.
- [11] J. Kuipers, "Tracking and determining orientation of object using coordinate transformation means, system and process," U.S. Patent 3 983 474, Sept. 26, 1976.
- [12] J. Kuipers, "Apparatus for generating a rotating electromagnetic field," U.S. Patent 4 107 858, Apr. 12, 1977.
- [13] M.R. Kraichman, *Handbook of Electromagnetic Propagation in Conducting Media*, 2nd ed. Washington, D.C.; Headquarters Naval Material Command, 1976. (USGPO stock no. 008-040-00074-5.)
- [14] R.L. Pio, "Euler angle transformation," *IEEE Trans. Automat. Contr.*, vol. AC-11, pp. 707-715, Oct. 1966.
- [15] F.H. Raab, "Remote object position locator," U.S. Patent 4 0054 881, Oct. 18, 1977.
- [16] J. Kuipers, "TWO-WAY, a position and orientation measurement system," *Proc. MTS IEE OCEANS '77*, pp. 38E-1 to 38E-13, La Jolla, Calif., Oct. 1977.



Frederick H. Raab (S'66—M'72) received the B.S., M.S., and Ph.D. degrees in electrical engineering from Iowa State University, Ames, in 1968, 1970, and 1972, respectively.

He then worked for Cincinnati Electronics Corporation for 3½ years in the areas of high-efficiency power amplifiers and search-and-rescue navigation. Since joining Polhemus Navigational Sciences, Inc., in 1975, he has been involved with terrestrial applications of Loran-C and the development of an electromagnetic system for locating trapped mine workers. His professional interests include communications, navigation, signal processing, and power amplifiers.

Dr. Raab is a member of the Institute of Navigation, the International Omega and Wild Goose Associations, Eta Kappa Nu, and Sigma Xi.



Ernest B. Blood studied physics at Lowell Technology Institute, received the B.S.E. degree in aerospace engineering from the University of Michigan in 1966, and did graduate work there in aerodynamics.

He was then employed by Lockheed Aircraft where he participated in simulation, modeling, and prediction of aerodynamic and performance characteristics of various aircraft. He joined Polhemus Navigation Sciences, Inc., in 1970 and has participated in numerous radio navigation studies of the Loran-C, Decca, Omega, and Transit Systems. As head of the Computer Sciences Group, he is responsible for the design of the software and processors used in the SPASYN systems.



Terry O. Steiner received the B.S. degree in physics from Case Institute of Technology, Cleveland, Ohio, in 1970 and is currently doing graduate work in physics at the University of Vermont.

He served in the U.S. Air Force for 4 years where he was involved in RF environmental studies and in establishing personnel exposure criteria. Since joining Polhemus Navigation Sciences, Inc. in 1975, he has been involved in the design of SPASYN three-axis source and sensor arrays.



Herbert R. Jones received the B.S.E.E. degree and (while a National Science Foundation scholar) the M.S.E.E. degree from the University of Vermont in 1968 and 1972 respectively. He was a Ph.D. candidate at the University of Vermont where he tutored courses in electric and magnetic fields, solid-state physics, and computer logic.

Since joining Polhemus Navigation Sciences, Inc., in October 1977, he has been charged with the design of 16-bit processor-to-resolver, serial-digital interfaces, and high-precision analog signal conditioning circuitry for a number of SPASYN system variations. In addition to his circuit design tasks, he was project engineer/program manager on a number of SPASYN system installations and has been heavily involved in developing SPASYN calibration and alignment procedures.